Defence Research and Development Canada
Recherche et développement pour la défense Canada

CAN UNCLASSIFIED

DRDC | RDDC
technologysciencetechnologie

On the determination of the shock and steady state parameters of gelatine from cylinder impact experiments

Dennis Nandlall
DRDC – Valcartier Research Centre

Augustin Gakwaya
Département Génie Mécanique, Université Laval

International Journal of Impact Engineering, Elsevier, Vol 116, pp. 22–33

Date of Publication from Ext Publisher: May 2018

Defence Research and Development Canada

External Literature (P)
DRDC-RDDC-2018-P069
May 2018

CAN UNCLASSIFIED

Canada

IMPORTANT INFORMATIVE STATEMENTS

International Journal of Impact Engineering 116 (2018) 22–33

Contents lists available at ScienceDirect

International Journal of Impact Engineering

journal homepage: www.elsevier.com/locate/ijimpeng

On the determination of the shock and steady state parameters of gelatine from cylinder impact experiments

D. Nandlall[a,*], A. Gakwaya[b]

[a] Defence Research and Development Canada, 2459 boul. de la Bravoure, Quebec City, Quebec, G3J 1X5, Canada
[b] Département Génie Mécanique, Université Laval, 1065 Avenue de la Médecine, Québec City, Québec, G1V 0A6, Canada

ARTICLE INFO

Keywords:
Low strength material impact
Soft body material impact
Shock pressure of gelatine impact
Bird strike
Human surrogate materials

ABSTRACT

For a soft body projectile striking a target or the shock loading of a soft body material, the determination of the interface shock pressure, shock speed and applied steady state pressures is important but has been hindered by technical challenges even with the use of sophisticated embedded pressure sensors in the target surface. Difficulties interpreting the results render the accuracies sometimes questionable or impossible to reproduce. Here we propose a simple impact experiment using a force sensor and an analysis procedure to derive the interface pressure from the force/time history. The results are compared to those obtained from shock Hugoniot and penetration equations. We came upon the presence of a dynamic pressure that is significantly higher than the expected stagnation pressure. This method could be used to determine and characterise the shock and steady state pressures of a wider range of materials under impact and shock loading conditions.

1. Introduction

Low strength materials such as water, gelatine, rubber, wax or even emulsions are used for a broad range of applications involving impact and shock loading conditions. Apart from being used as shock absorbers or in energy dissipating systems, these materials, such as gelatine and rubber, are used as surrogates for human body tissues, organs, biological liquids, animals and birds to examine the effects that may occur due to impact or shock. Examples range from the use of extra-corporeal shock wave lithotripsy [1] in the non-invasive disintegration of urinary tract stones or ultrasounds for the denaturing of deep seated cancerous cells [2] to the studying of trauma [3] caused to the human body due to impact or shock loading or the damage to aircraft structures due to bird impact [4–12]. In all these examples, the shock and steady state pressures are important loading parameters that are needed to understand the response of the materials and these parameters are normally measured at the impactor/target interface. In an impact problem, especially in the case involving a soft body material, the simultaneous deformation of the projectile and target makes uncoupling the response of each material very difficult so to decouple and understand the responses, studying cylinders made out of a particular material striking rigid targets provides researchers with a very useful means to characterise a material under shock loading condition whether it is used as an impactor as in the case of a bird strike problem or a target as in the case of a human surrogate struck by a projectile. Studies [13–19] on the deformation of solids by liquid impact at supersonic speeds examined flat-ended cylinders striking a rigid target and described the interface pressure as the water hammer pressure, $P = \rho c_0 u_0$ where ρ is the density, c_0 is the wave speed and u_0 is the impact velocity. Further studies [24–28] on the issue have shown that the water hammer equation pressure works well only for low velocity impact but for higher velocities, c_0 must be replaced by the shock velocity, U_s, to get what is called the shock or Hugoniot pressure, $P_h = \rho U_s u_0$. These studies have all shown that when a projectile strikes a target (Fig. 1) a shock is generated at the center of the projectile and propagates towards the outside surface and on reflection, forms release waves that propagate towards the center at a lower pressure which causes the material to flow. The pressure at the interface begins to decrease and after several reflections the projectile flow will approach a steady state condition where the pressure becomes the stagnation pressure, $P_{stagnation} = \frac{1}{2}\rho u_0^2$. Many studies [4,7–9,13–24] have validated this theory of the shock and steady state regimes govern, respectively, by the shock Hugoniot and the steady state pressure and from the literature cited there is general agreement on this. Many researchers [4–12] in measuring these pressures use pressure transducers embedded in the surface of the target where the projectile first strikes. However, in all the work cited for soft body impact, although good shock and steady state pressure results are obtained, there are many difficulties, such as the limitation of the pressure gauges that rendered the accuracies of the data sometimes being questionable or difficult to reproduce.

* Corresponding author.
E-mail address: dennis.nandlall@drdc-rddc.gc.ca (D. Nandlall).

https://doi.org/10.1016/j.ijimpeng.2018.02.001
Received 24 October 2017; Received in revised form 31 January 2018; Accepted 6 February 2018
Available online 08 February 2018

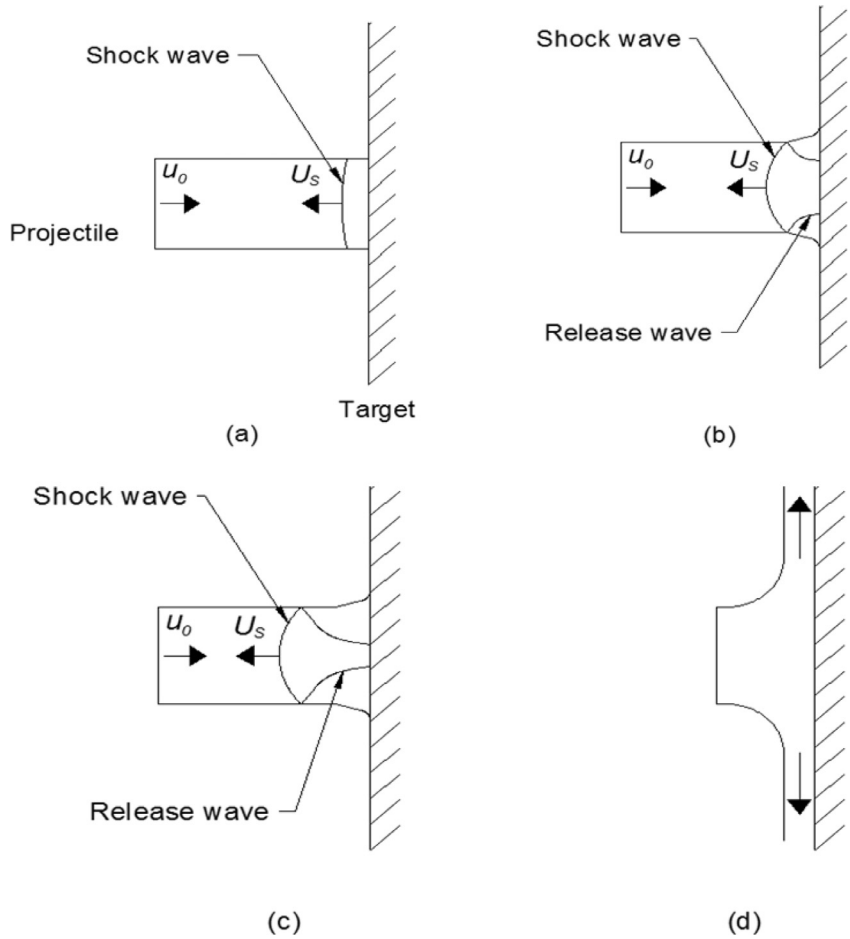

Fig. 1. Illustration of the four stages of a soft body projectile striking a rigid target.

Studies [4–6,10,11] spanning the last three decades have highlighted these limitations and this led us to re-look at the issues of the impact problem and examine whether reliable shock and steady state pressures could be obtained from a simple more repeatable experiment that could be used to examine a broad range of soft body materials.

2. Experiments

Here we propose using a force ring transducer, instead of a pressure gauge, sandwiched between a rigid target disc and a clamped support plate to determine the interface pressure using the force-time history. An air gun impact facility (Fig. 2(a)) was used to conduct the experiments. The air gun itself consisted of a 1.8-m long, 40-mm diameter launch tube that is coupled to a compressed air reservoir. The pressure of the air in the reservoir determines the exit velocity of the projectile. A phototron high speed camera recording at 20,000 frames/s, was used to record the projectile release from the launch package, its flight to and interaction with the target. The data acquisition system integrated with the gun firing mechanism, was used to trigger the camera and acquire the force history. To launch projectiles with the air gun, a sabot (Fig. 2(b), Appendix A.2 - Sabot development and Appendix B - Fig. B. 1) was required to hold the penetrator in place during its travel in the launch tube and then stripped away before striking the target. The basic projectile (Fig. 2(b)) was a 28-mm cylindrical 10% gelatine rod with a hemispherical tip and a nominal length of 102 mm and was prepared using a standard 10% gelatine recipe [1,9] (Appendix A.1 - Gelatine preparation). The target was a 120-mm diameter, 19-mm thick steel disc with a solid 28-mm diameter cylindrical support at the center that was attached to the center of a 330-mm, 35-mm thick square steel plate sandwiching a force ring sensor (Fig. 2(c)). The force transducer used was a PCB Piezotronics Quartz Force Ring Sensor Model 207C (Fig. 2(d)) with a force measurement of up to 445 kN and a sensitivity of ± 1.5%.

3. Results - experimental data reduction and discussion

Of the many tests conducted, four at different impact velocities, 74, 105, 115 and 119 m/s, were chosen to conduct the analysis. Fig. 3 shows a sequence of the projectile/target interaction in time for the 119 m/s impact velocity case, starting with the projectile striking the target until it was completely eroded. A closer look at the sequence of pictures reveals that as the material goes from the initial shock phase and into deformation due to the large compressive forces, the front of the projectile mushrooms and then there appears to be considerable shearing and fissuring of the material into fragments and subsequently entering into the radial flow which remains parallel to the target. This tearing or shearing of the material into fragments are also very evident from the pieces of the gelatine (Appendix B - Fig. B. 2) gathered after the test. This appears to be different than the flow of water or a liquid striking the target. The solid line of the force histories shown in Fig. 4 are the raw force data as acquired from the tests and significant oscillations were observed in the results. A Fourier transform [21] on the

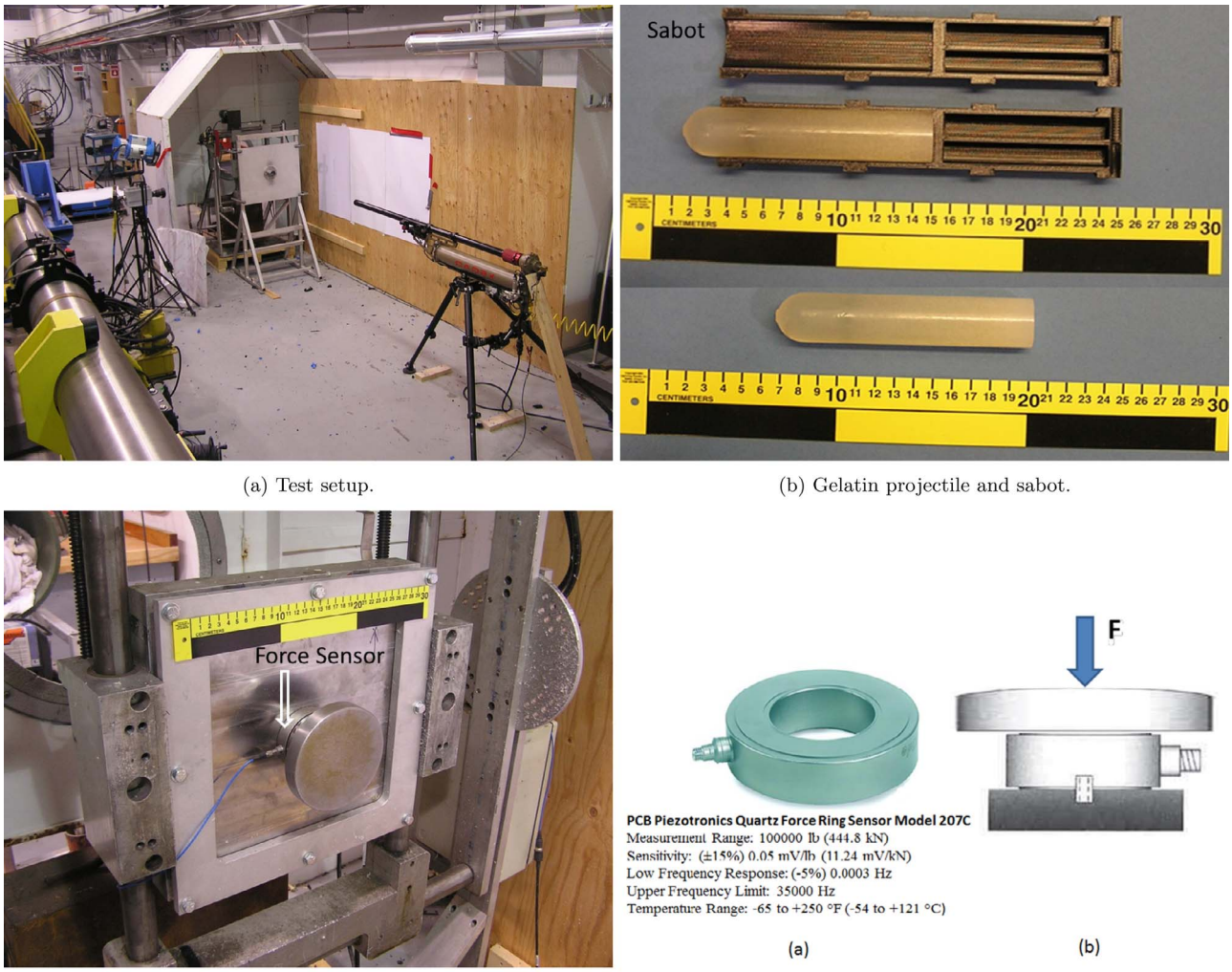

(a) Test setup.

(b) Gelatin projectile and sabot.

(c) Target with force sensor installed.

(d) Force sensor and configuration.

Fig. 2. Air gun, gelatine projectile, target and force transducer setup.

force time data (Appendix B - Fig. B. 3) revealed the presence of two frequencies one at 2000 Hz and the other at 15,000 Hz and whose amplitudes changed significantly with the impact velocity. A manual roving hammer test was conducted, striking different parts of the target and its supporting structure and the two frequencies were generated only when either the target disc or supporting plate was struck. To confirm the source of these frequencies, the natural frequencies of the two plates were calculated using the Bessel function solution [22–24] to the wave equation for the vibrations of plates, $f = \frac{1}{2\pi}\frac{\lambda^2}{a}\sqrt{\frac{D}{\rho h}}$ where $D = \frac{Eh^3}{12(1-\nu^2)}$ is the flexural rigidity. ρ is the density, E is the Young's modulus, h is the plate thickness, and ν is the Poisson's ratio. a is either the diameter of the disc or the length of plate. λ^2, the non dimensional Bessel coefficient [26–28] for the first mode, equals 36 for a clamped square plate and 6.25 for an annular disc clamped at the center. The target disc was treated as an annulus [29], free on the outside and clamped on the inside over a 28-mm diameter area where it is attached to the square plate sandwiching the Force ring sensor. The frequencies calculated were very close to the frequencies found in the Fourier transform of the force time data confirming that these two superimposed frequencies were from the free vibrations of the target plates (Appendix B - Fig. B. 3). The Savitsky–Golay [30,31] filter that tends to preserve key data features such as peak height, width and zero phase shift so that the signals are not shifted, was used to remove the 15,000 Hz frequency whereas a Butterworth band-stop filter was used to remove the lower 2000 Hz frequency. The dashed curves in Fig. 4 show the filtered data. The force caused by the shock pressure is taken to be the maximum force arrived at just after the steep rise which is essentially the highest peak in the raw data history. The remainder of the force-time curve would indicate the steady state loading of the target until the projectile has completely eroded or rebounded. In the 74 m/s impact velocity case, two peaks in the force-time curve could be observed. The video showed that the projectile broke into two pieces before impact and essentially there were two impacts one after the other occurring at the target. The impact velocity of the second part may have been be a little lower than 74 m/s given that it seemed to have struck the back end of the first part of the projectile before coming into contact with the target. The results, therefore, appears to be

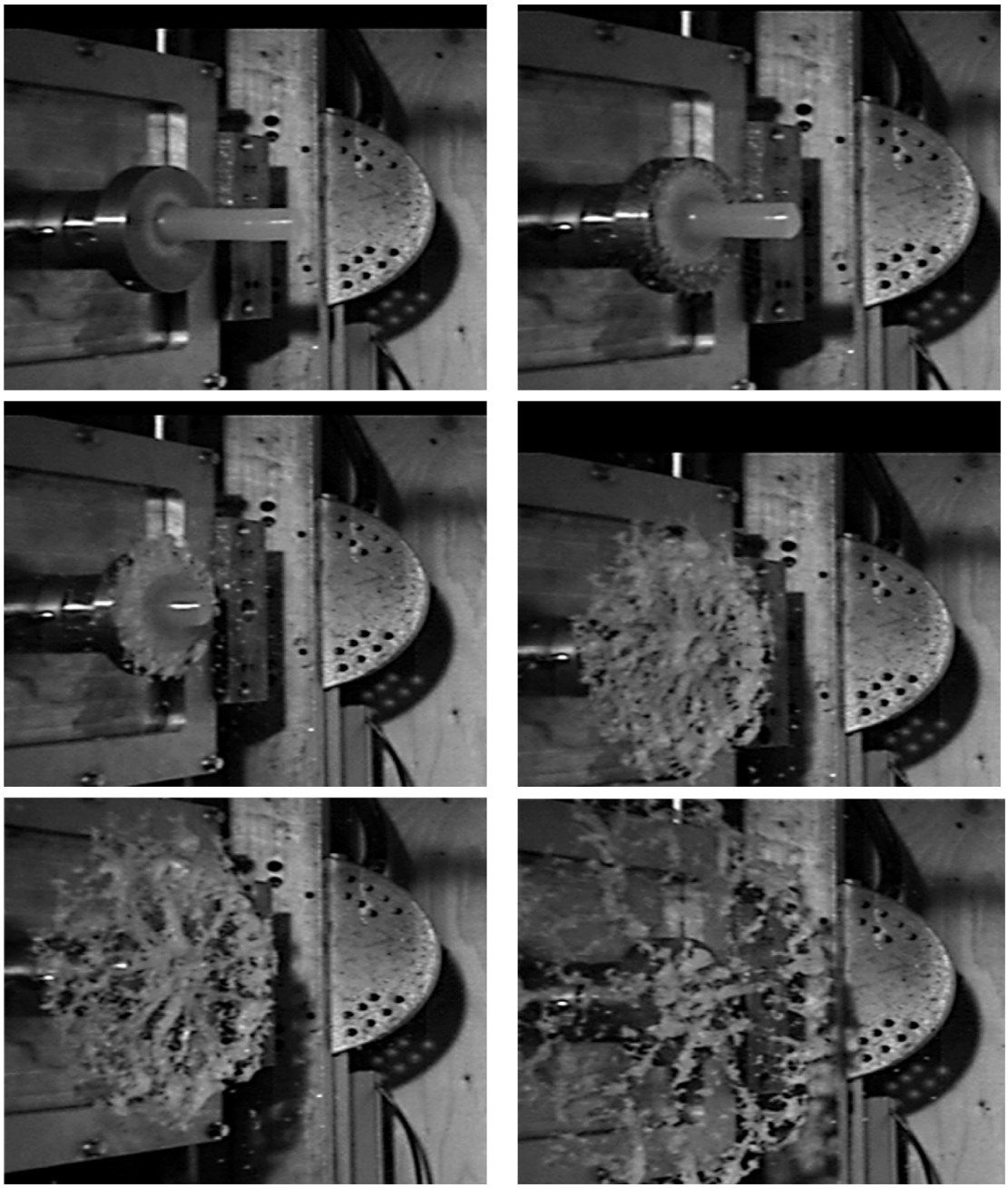

Fig. 3. Time sequence snapshots of the projectile/target interaction for the 119 m/s impact velocity test case.

consistent with those of the other tests. In an impact problem, when a pressure is applied, based on the difference in the impedances of the two materials, part of the pressure is transmitted and the part is reflected [1,32,33]. It is known [1] that the fraction that is transmitted is given by the transmission coefficient, T_t, as

$$T_t = \frac{2Z_2}{Z_1 + Z_2} \tag{1}$$

whereas, for the reflected fraction, the reflection coefficient T_r, is given by

$$T_r = \frac{Z_2 - Z_1}{Z_1 + Z_2} \tag{2}$$

where $Z_1 = \rho_1 U_{s1}$, $Z_2 = \rho_2 U_{s2}$ are the shock impedances for medium 1 and 2, respectively, and U_{s1} and U_{s2} are the corresponding shock speeds which are obtained from the $U_s - u_p$ shock Hugoniot (Appendix A.3 - Shock pressure solution and Appendix B - Fig. B. 4)

$$U_s = c_0 + su_p \tag{3}$$

where c_0 is the acoustic velocity and s is the slope. $T_t + T_r = 1$ and because of this condition, medium 2 would be assigned to the steel target

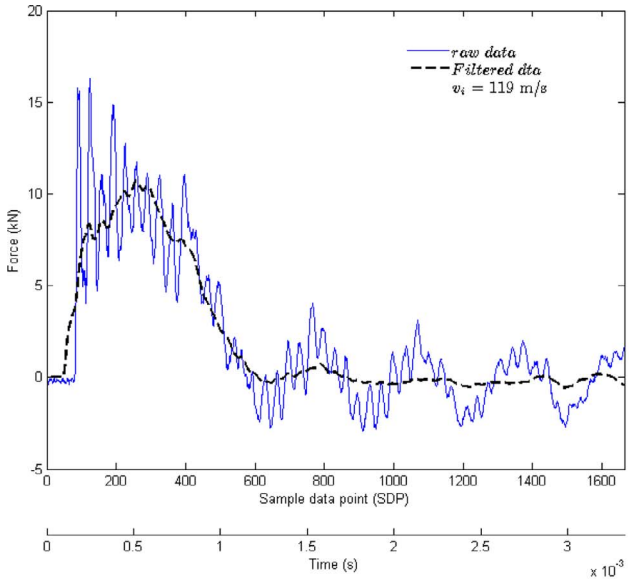

(a) Force history $v_i = 119$ m/s.

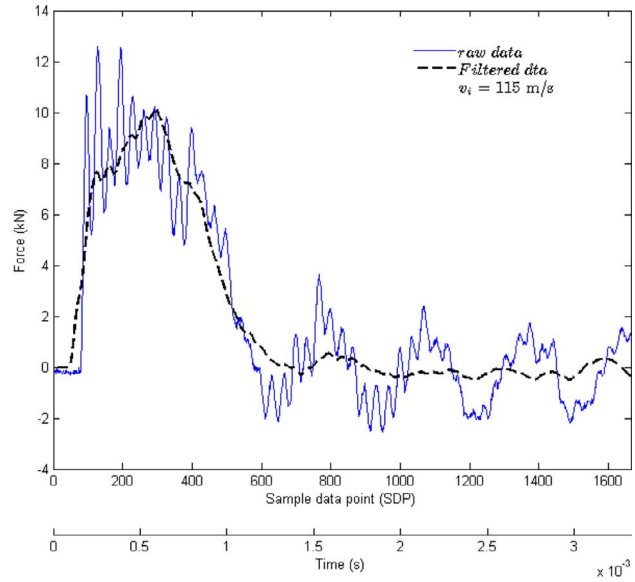

(b) Force history $v_i = 115$ m/s.

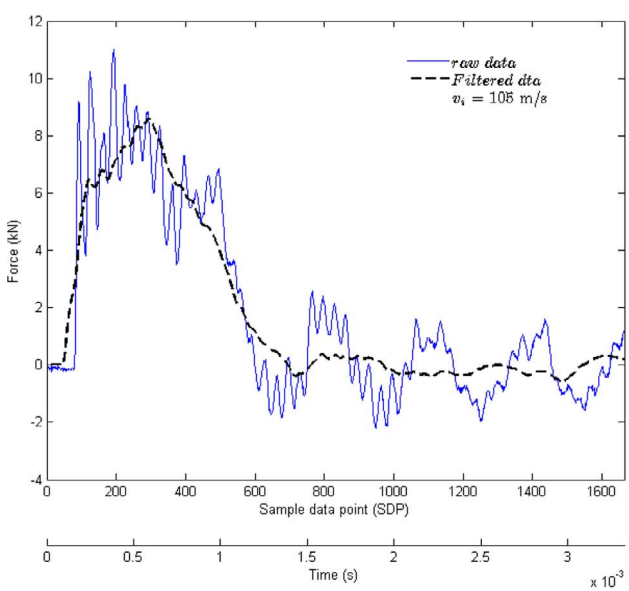

(c) Force history $v_i = 105$ m/s.

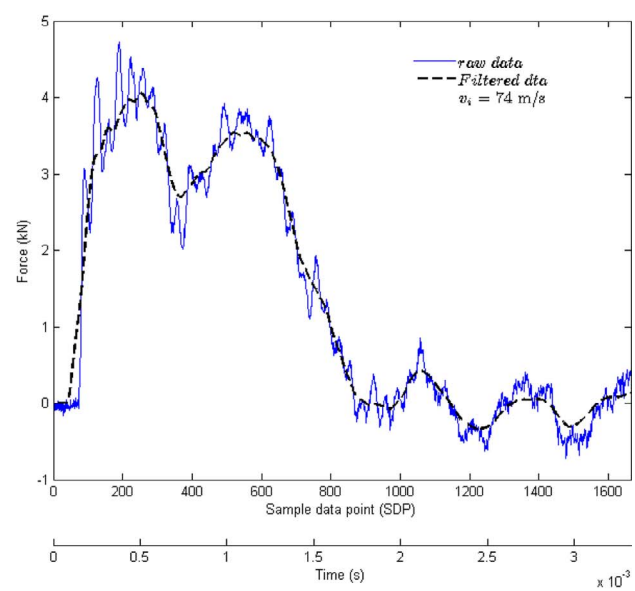

(d) Force history $v_i = 74$ m/s.

Fig. 4. Raw and filtered force history as a function of sampling data point and time.

Table 1
Properties/parameters required to determine shock and particle velocities in gelatine [3] and steel [32].

Property/parameter	Gelatine	Steel
Density, ρ (kg/m^3)	1030	7800
Acoustic velocity, c_0 (m/s)	1445	5800
Shock parameter, s	1.9	1.434

which is the higher impedance material of the two materials that are in contact and medium 1 would be assigned to the gelatine. Thus, the amplitude of the force measured would be caused by the transmission fraction, T_t, of the original pressure applied at the projectile/target interface. The shock properties [3,32] required to calculate the shock speeds in the gelatine and steel are given in Table 1.

Table 2 shows a summary of the important results for the four tests conducted. For each impact velocity, u_{0p} or v_i, the corresponding interface particle velocity, u_p was calculated (Appendix A.3 - Shock pressure solution, Eq. (A.6)). This was then used to calculate the shock speeds, U_{steel} and $U_{gelatine}$ using Eq. (3). The shock speeds were then used to calculate T_r and T_t using Eqs. (1) and (2). Knowing the force, F_h (Table 2), the transmission coefficient is used to determine the interface shock pressure, P_{he} (Table 2). For example, for the case where $v_i = 119$ m/s, $T_t = 0.073$. Thus, 7.3% of the of the interface shock pressure was transmitted. Scaling this to 100% and dividing by the cross sectional area of the projectile, 616 mm^2, an interface pressure, P_{he}, of 191 MPa

Table 2
A summary of results giving the impact velocity, v_i, the interface particle velocity, u_p, shock speed in steel target and gelatine projectile, U_{steel} and $U_{gelatine}$, the transmission and reflective coefficients, T_t and T_r, the filtered experimental shock force, F_h, the experimentally derived shock pressure P_{he} and the theoretical shock pressure, P_{ht}. t_{exp} and t_{pr} are, respectively, the experimental and predicted projectile/target interaction time.

v_i (m/s)	u_p (m/s)	U_{steel} (m/s)	$U_{gelatine}$ (m/s)	t_{exp} (ms)	t_{pr} (ms)	T_r	T_t	F_h (kN)	P_{he} (MPa)	P_{ht} (MPa)
119	3.8	5806	1663	0.87	0.88	0.927	0.073	8.59	191	196
115	3.8	5806	1655	0.90	0.89	0.927	0.073	7.73	174	189
105	3.8	5805	1637	1.00	0.98	0.923	0.072	6.80	154	171
74	2.7	5804	1581	1.40	1.38	0.931	0.069	4.05	95	116

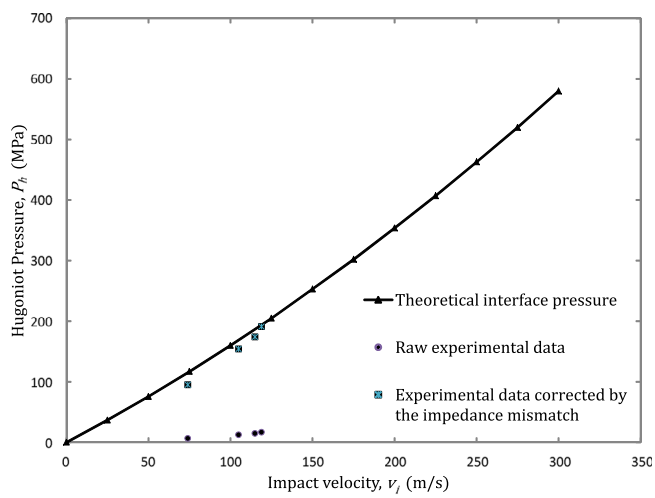

Fig. 5. Comparison of the calculated experimental shock pressure with the theoretical value as a function of impact velocity.

was obtained. Fig. 5 shows a comparison of the theoretical, $P_{ht} = \rho U_s v_i$ (Appendix A.3 - Shock pressure solution, Eq. (A.7)) and the derived experimental interface shock pressures P_{he}, as a function of impact velocity and good agreement is obtained.

For the duration of the projectile/target interaction (Table 2) there is very good agreement between the measured time, t_{exp} and the predicted value $t_{pr} = \frac{l}{v_i}$ obtained from the Alekseevskii–Tate equations [25,26,34,37,38] (Appendix A.4- Steady state solution, Eq. (A.13)). This is an indication that the erosion rate and the application of the pressure on the target are consistent with the measured force. With respect to the steady state interface pressure, in accordance with the penetration equations (Appendix A.4 - Steady state solution, Eqs. (A.9) and (A.14), it was established that if Y_p, the projectile dynamic strength, is assumed to be negligible then the steady state pressure at the interface would be $P_{stagnation} = \frac{1}{2}\rho v_i^2$. However, interpretation of the experimental results does not appear to indicate this. Consider the experimental results shown in Fig. 6, $P_{stagnation}$ is plotted on the same axes as the experimentally derived pressure-time curves.

Examination of the two curves reveals that the $P_{stagnation}$ is much lower than the experimentally derived pressure by an amount, ΔP. This indicates the presence of a dynamic pressure that the projectile material is applying to the target and is of the order of the shock pressure. This observation could be explained in accordance with the penetration equations (Appendix A.4 - Steady state solution, Eq. (A.14)). If Y_p is taken into consideration [35], then setting $Y_p = \Delta P$, Y_p could be termed as a dynamic pressure applied by the gelatine and it is impact velocity dependent. We know that this could not be due alone to the strength of the projectile as is often used in the case of other solid penetrators materials because studies [40,41] have shown that the fracture strength of gelatine at reasonably high strain rates is between 1 and 2 MPa so there must other phenomena occurring. A close observation of the projectile/target interface provides one explanation. It appears that the gelatine material in the mushrooming region of the projectile is undergoing severe compression enough to cause a significant increase in the bulk modulus which in turn manifests itself in a localised increase in the bulk density enough to cause a significant rise in the pressure applied to the target. This continues for about half way through the length of the projectile interaction with the target after which the interface pressure dropped linearly to zero as the projectile erodes away. This argument of the compression in the impact region resulting in presence of this dynamic high pressure could be substantiated by similar observations made by Field et al. [16,17] and other studies [13–24] that examined the impact of liquid and water-gelatine mixtures on solid structures only in this case we do have a quantitative measure of this dynamic high pressure present at the interface. Fig. 7 shows the maximum ΔP as a function of impact velocity and a quadratic fit to the data indicates that the peak dynamic strength pressure at the interface rapidly increases with impact velocity.

4. Conclusion

A simple cylinder impact test was used to examine the impact process of a soft body material projectile made of 10% gelatine, striking a rigid target attached to a quartz force ring sensor instead of a usually used pressure sensor. The shock and steady state pressures were determined from the force-time histories. In an effort to obtain accurate and reproducible results, the force time curves were examined to identify frequencies that were present in the results and may be coming from the natural vibrations of the various parts that make up the target. The Bessel function solutions for the wave equation applied to the free vibration of plates were used to examine the vibrations of the various plates in the target assembly and once identified and determined were removed using the Savitsky–Golay filter. Using the shock Hugoniot relations and the conservations equations, the theoretical shock pressure relation was developed for the shock pressure at the projectile/target interface. The shock pressures derived from the experimental force/time histories were in very good agreement with the theoretical values predicted by the shock Hugoniot. The Alekseevskii–Tate penetration equations were used to determine the steady state pressure at the projectile/target interface and the duration of the interaction between the projectile and target. The equations predicted very well the duration of the interaction. However, the measured value of the steady state pressure was in discordance with the expected stagnation

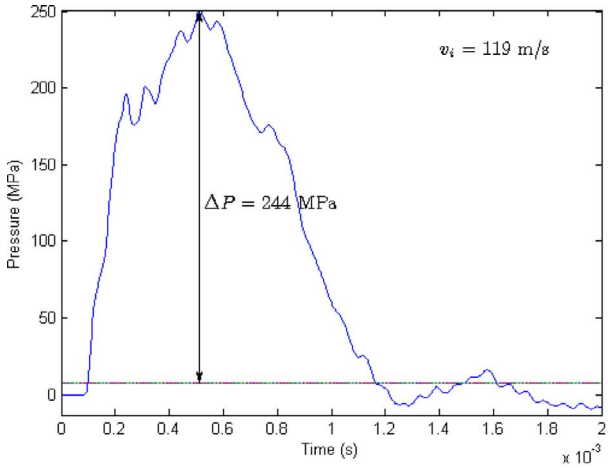

(a) Dynamic interface pressure ΔP, for $v_i = 119$ m/s.

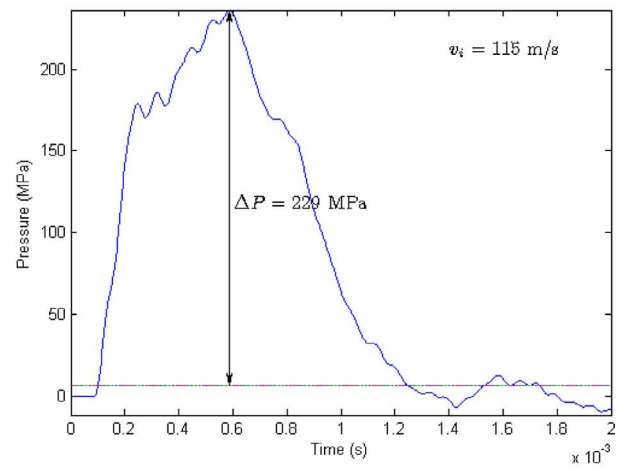

(b) Dynamic interface pressure ΔP, for $v_i = 115$ m/s.

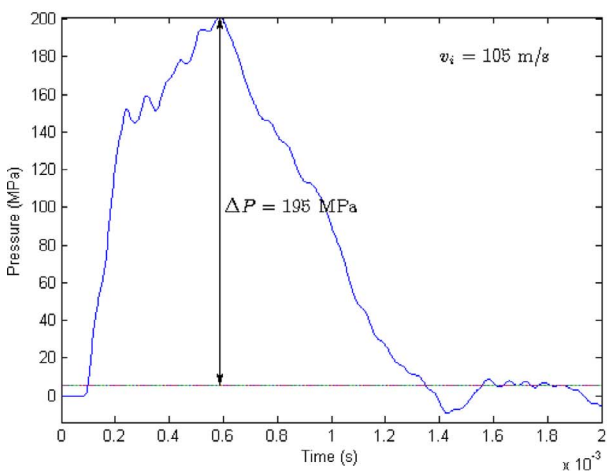

(c) Dynamic interface pressure ΔP, for $v_i = 105$ m/s.

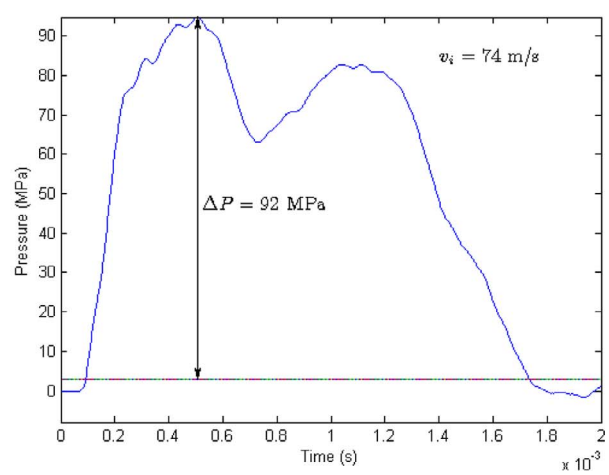

(d) Dynamic interface pressure ΔP, for $v_i = 74$ m/s.

Fig. 6. Dynamic interface pressure, ΔP, as a function of time.

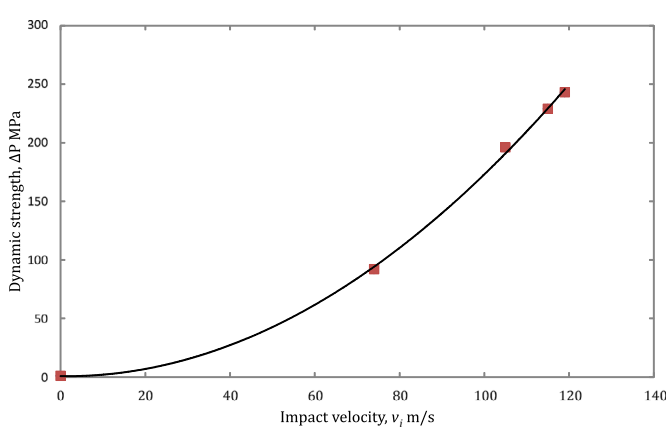

Fig. 7. Maximum interface dynamic pressure, ΔP, as a function of time.

pressure, $P_{stagnation} = \frac{1}{2}\rho v_i^2$. We came upon the presence of a dynamic pressure which when interpreted in accordance with the Alekseevskii–Tate equations, suggests that the material dynamic strength manifested from the compression of the gelatine material caused a change in the bulk modulus or density and, thus, the increased pressure. A quantitative measure of this dynamic strength as a function of time was obtained and it is dependent on the impact velocity. Given the significant value of this dynamic pressure, it may be necessary to take this into account when these materials are used in shock loading and impact scenarios.

Acknowledgments

This work was supported by Defence Research and Development Canada (DRDC) through the Project: 02AB 1.2.1 - I/O ST02Ab0201GV Soldier Systems Effectiveness (SoSE) project and a collaboration with the Consortium for Research and Innovation in Aerospace in Quebec (CRIAQ/NSERC) through Project: COMP 410 their bird impact project with Université Laval. The support of both projects is gratefully acknowledged. In particular, the author, DN, would like to express his sincere thanks to G. McIntosh for the many hours of discussion on impact physics without which we would not have achieved as much. A special thank you to S. Nandlall for introducing the Savitsky–Golay filtering method without which processing the experimental results would have proven much more difficult. Earnest thanks to N. Viel for manufacturing the sabot and to D. Leclerc for his skill and knowledge in conducting the experiments and surmounting the challenges in launching gelatine projectiles.

Appendix A. Methods

A1. 10% gelatine preparation

The gelatine projectiles were prepared using a standard recipe [4,10,11]. The ingredients were 1000 g cold water, 100 g ballistic gelatine powder, 25 g sodium carboxy methyl cellulose(CMC), 6 g aluminum acetate basic (AAB), 4 drops of cinnamomum zeylanioum (cinnamon). The procedure was to mix the cold water and the gelatine, wait 5 min and then heat up the mixture to 45°C. 1050 g of the gelatine mixture was then poured into a blender and the mixture of CMC and AAB was added. The drops of cinnamon were added and the mixture was blended at the lowest speed for 3–5 s. It was then poured into pre-warmed molds and refrigerate for 36 h. Compressed air was used to remove the gelatine projectiles from the molds. Random samples across the length of two projectiles from every batch of gelatine made were used to verify the density and it was found consistently to be 1030 kg/m^3.

A2. Sabot development

A special sabot (Appendix B, Fig. B. 1) was designed and provides a unique efficient and inexpensive method to launch a soft body projectile. It was made of thermoplastic resin Acrylonitrile-Butadiene-Styrene (ABS) using additive manufacturing. This particular design allowed for the penetrator back end to be forward displaced in the sabot. If the projectile back end sits at the back of the sabot as it leaves the launch tube the compressive forces of the gelatine push the back end of the sabot apart causing the front ends to approach each other forming a pivot in front of the projectile. This provides an opportunity for the sabot to pass through the sabot trap and to strike the target. Displacing the projectile towards the front allows the compressive forces to start pushing the sabot apart while the back end is still in the launch tube and as it exits the aerodynamic forces continue to push the sabot sections apart and are subsequently stopped by the sabot trap while allowing the projectile to pass (Appendix B, Fig. B. 1(d)). The ribs around the circumference stiffen the sabot to avoid buckling in the launch tube.

A3. Shock pressure solution

When a shock is generated, the shock front in the material moves with a velocity U_s which is material dependent. The material behind a shock front moves with a particle velocity, u_p. The $U_s - u_p$ Hugoniot shown in Eq. (3) is normally derived experimentally [3,32] and have shown that for most materials it is a linear relationship (Appendix B, Fig. B. 4). If the $U_s - u_p$ data are available, as it is for most materials, the interface particle velocity and shock pressure could be obtained by using Eq. (3) in conjunction with the conservation equations for mass, momentum and energy given, respectively, by

$$\frac{\rho_1}{\rho_0} = \frac{\nu_0}{\nu_1} = \frac{U_s - u_0}{U_s - u_1} \tag{A.1}$$

$$P_1 - P_0 = \rho_0(P_1 u_1 - P_0 u_0)(U_s - u_0) \tag{A.2}$$

$$e_1 - e_0 = \frac{(P_1 u_1 - P_0 u_0)}{\rho_0(U_s - u_0)} + \frac{1}{2}(u_1^2 - u_0^2) \tag{A.3}$$

where the subscripts 0 and 1 are used to indicate conditions ahead and behind the shock front. Consider the impact problem described in Fig. 1 with the projectile moving from left to right for convenience. Combining Eq. (3) with the momentum Eq. (A.2), the $P - u$ Hugoniots [32,33], Eqs. (A.4) and (A.5), are obtained, respectively, for the right hand shock moving in the target, $u_p > u_0$, and the left hand shock moving in the projectile, $u_p < u_0$.

$$P_{ht} = \rho_{0t} c_{0t}(u_{1t} - u_{0t}) + \rho_{0t} s_t (u_{1t} - u_{0t})^2 \tag{A.4}$$

$$P_{hp} = \rho_{0p} c_{0p}(u_{0p} - u_{1p}) + \rho_{0p} s_p (u_{0p} - u_{1p})^2 \tag{A.5}$$

where the subscripts t and p relate, respectively, to the projectile and target materials. The pressure and the particle velocity across the interface of both materials must be consistent to satisfy the conservations equations. Thus, equating these two equations (shown graphically in Appendix B, Fig. B. 5) and eliminating the pressure terms results in a quadratic equation for the interface particle velocity, u_p given by

$$\begin{aligned}(\rho_{0p} s_p - \rho_{0t} s_t) u_p^2 - \\ (\rho_{0p} c_{0p} + 2\rho_{0p} s_p u_{0p} + \rho_{0t} c_{0t} - 2\rho_{0t} s_t u_{0t}) u_p + \\ (\rho_{0p} c_{0p} u_{0p} + \rho_{0p} s_p u_{0p}^2 + \rho_{0t} c_{0t} u_{0t} u_{0t} - \rho_{0t} s_t u_{0t}^2) = 0\end{aligned} \tag{A.6}$$

Knowing the particle velocity provides three options to obtain the interface shock pressure either by Eq. (A.4) or (A.5) or by solving for the shock speed in Eq. (3) and then using the momentum equation(A.2) in which after the initial conditions are substituted, reduces to

$$P_h = \rho_0 U_s v_i \tag{A.7}$$

A4. Steady state solution

The steady state solution is obtained from the Alekseevskii–Tate [34–39] penetration equations

$$l\frac{dv_i}{dt} = \frac{-Y_p}{\rho_r} \tag{A.8}$$

$$\frac{1}{2}\rho_r (v_i - w)^2) + Y_p = \frac{1}{2}\rho_t w^2 + R_t \tag{A.9}$$

$$v_i = w - \frac{dl}{dt} \tag{A.10}$$

$$\frac{dP_n}{dt} = w \tag{A.11}$$

where v_i is the rod velocity, w is the penetration velocity, P_n is the penetration, l is the penetrator length, t is the time after impact, R_t is the target strength and Y_p is the penetrator strength. ρ_p and ρ_t are, respectively, the penetrator and target densities. Given that the penetration velocity, $w = 0$, Eq. (A.10) could be solved explicitly for the projectile erosion

$$\frac{dl}{dt} = v_i \tag{A.12}$$

which implies essentially that the projectile erosion rate, $\frac{dl}{dt}$ is simply equal to impact velocity, v_i and the flow of the material at the target/projectile interface is considered to be steady state. Performing this simple integration and rearranging the equation making t the subject of the formula gives

$$t = l/v_i \tag{A.13}$$

which is the time the projectile spends interacting with the target before being completely eroded. In Eq. (A.9), setting the penetration velocity and taking the usual strength terms [36–39] as the pressures, an equation of the form

$$P_{interface} = \frac{1}{2}\rho_r v_i^2 + Y_p \tag{A.14}$$

For the case where the projectile strength is negligible, then $Y_p = 0$ and

$$P_{interface} = \frac{1}{2}\rho_p v_i^2 \tag{A.15}$$

is obtained where $P_{interface}$ is referred to as the stagnation pressure that is often found in literature [4–20].

Appendix B. Supplementary material

The supplementary material consists of five additional figures. Although the paper as it is could be read well without compromising the basic understanding of the work, the supplementary figures could be most helpful if the reader would like to use the test method, reproduce the results, follow in more detail the data reduction and analysis or the development of the interface shock pressure using the shock Hugoniot. Fig. B.1 shows various views of a unique sabot design that was used to launch the gelatine projectile and could be useful for reproducing or manufacturing the sabot. Fig. B. 2 shows the gelatine fragments recuperated and could shed some light on the failure of the material especially if one is considering of numerically simulating the impact problem using a hydrodynamic finite element code. Fig. B.3 shows the Force history in the frequency domain obtained using the Fourier transform in Matlab[25] and it does show the influence of natural vibrations of the target plates on the Force-time curves as

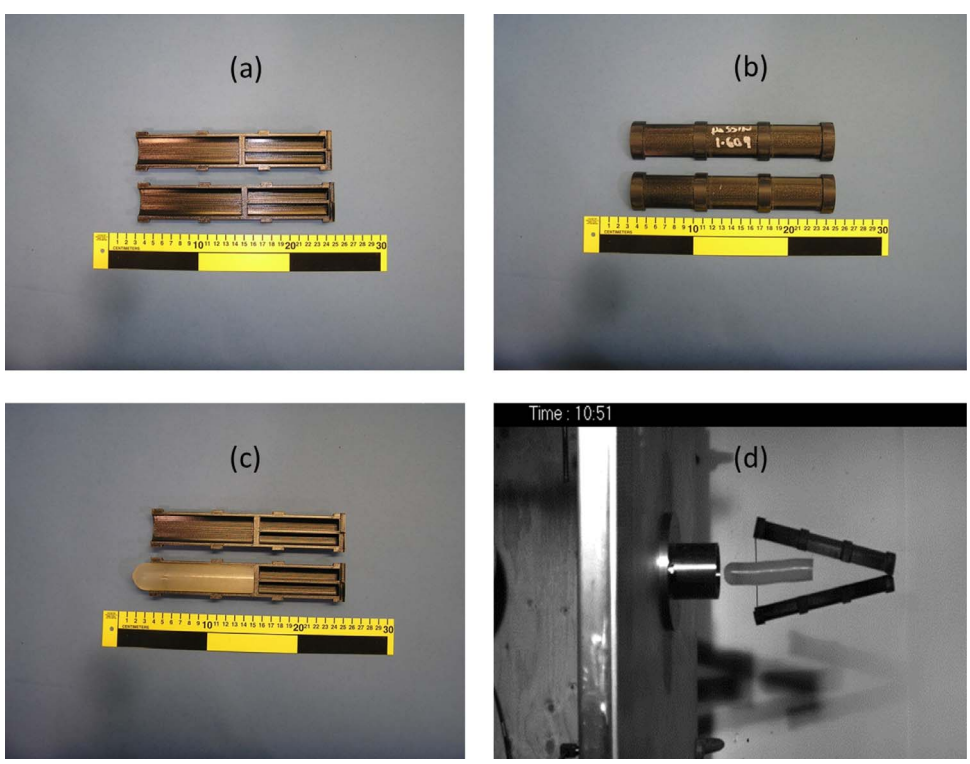

Fig. B.1. Various configuration views of the sabot: (a) the inside view. (b) a view of the outside (c) a view with the projectile placed in the sabot and (d) the separation of the projectile from the sabot just before passing through the sabot trap.

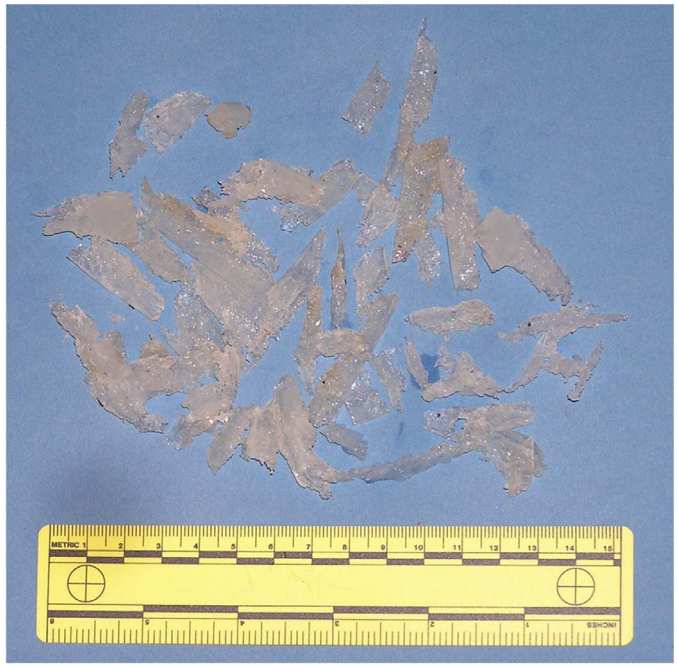

Fig. B.2. A collection of shredded gelatine fragments from the 119 m/s impact velocity test case.

a function of impact velocity. Fig. B. 4 shows a graphical representation of the $U_s - u_p$ shock Hugoniot, Eq. (3), that is used to obtain the shock speed for gelatine as a function of the particle velocity. Fig. B. 5 shows, for a particular impact velocity, a graphical solution for interface particle velocity by plotting the left hand and the right hand shock Hugoniots on the same axes. The intersection point of the two shock Hugoniots gives the interface particle velocity and shock pressure.

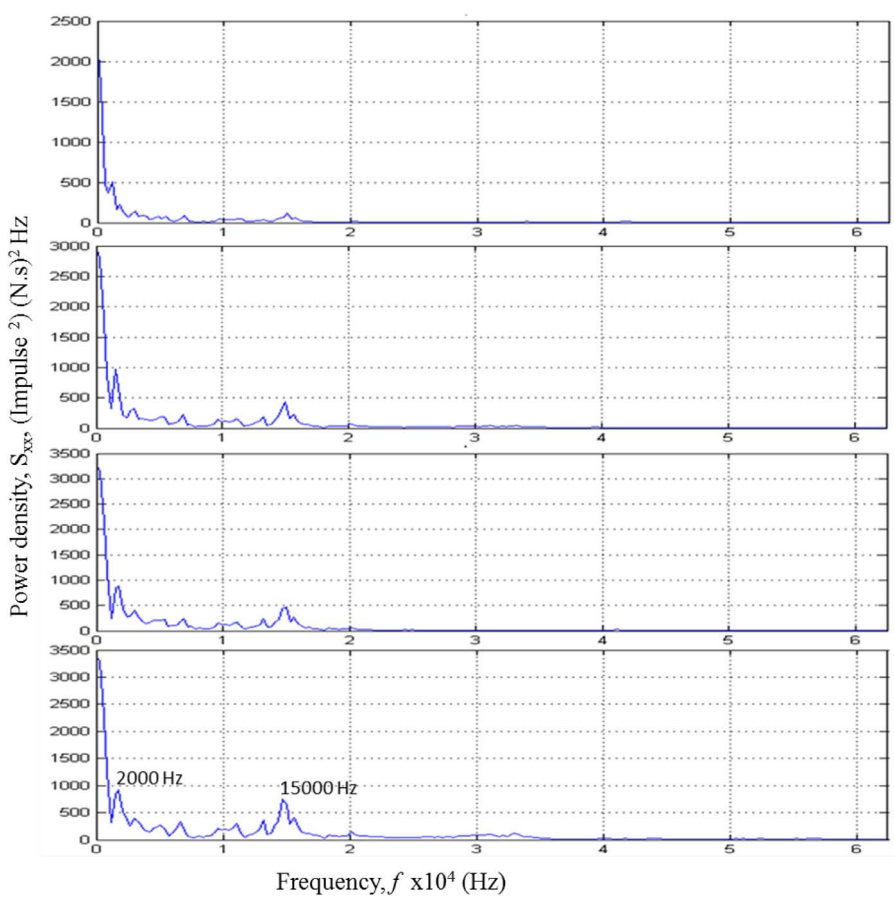

Fig. B.3. The force history in the frequency domain identifying frequencies present in the data.

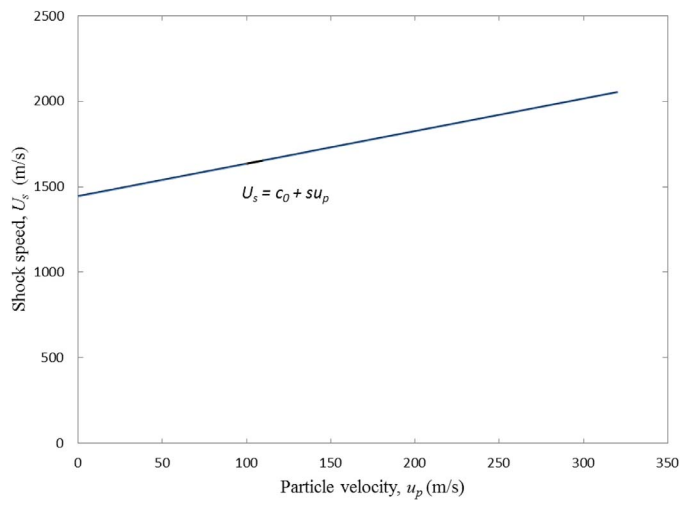

Fig. B.4. The $U_s - u_p$ shock Hugoniot for gelatine[3], $c_0 = 1445\,\text{m/s}$, $s = 1.9$.

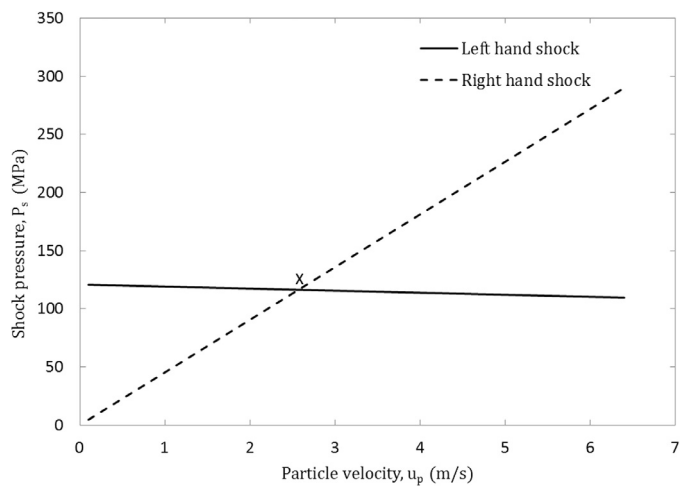

Fig. B.5. A graphical solution of simultaneously solving the left and right hand shock equations to obtain the interface shock pressure (point X) for a particular impact velocity, v_i.

Appendix C. Supplemetary material

Supplementary material associated with this article can be found, in the online version, at 10.1016/j.ijimpeng.2018.02.001.

References

[1] Cleveland RO, McAteer JA. Physics of shock-wave lithotripsy. Smith's textbook of endourology. 3rd 1. Wiley-Blackwell; 2012. p. 527–58.
[2] Nandlall SD. Monitering cell and tissue damage during ablation by high-intensity focussed ultrasound. Doctor of philosophy thesis University of Oxford, Oxford, UK; 2011.
[3] Gojani AB, Ohtani K, Takayama K, Hosseini SHR. Shock Hugoniot and equations of states of water, castor oil and aqueous solutions of sodium chloride, sucrose and gelatine. Shock Waves 2016;26(1):63–8.
[4] Wilbeck JS. Impact behavior of low strength projectiles. Wright-Patterson Air Force Base, Dayton, OH; 1978. Technical report afml-tr-71(2).
[5] Heimbs S. Computational methods for bird strike simulations: a review. Comput Struct 2011;89(23–24):2093–112.
[6] Hedayadti R, Sadighi M, Strike B. An experimental, theoretical and numerical investigation. Woodhead publishing in mechanical engineering. Elsevier, Cambridge, UK; 2016.
[7] Barber JP, Taylor HR, Wilbeck JS. Characterization of bird impacts on a rigid plate: part 1. Air Force Flight Dynamics Laboratory, OH; 1975. Technical report affdl-tr-75-5.
[8] Barber JP, Taylor HR, Wilbeck JS. Bird impact forces and pressures on rigid and compliant targets. Air Force Flight Dynamics Laboratory, OH; 1978. Technical report affdl-tr-77-60.
[9] Wilbeck JS, Barber JP. Bird impact loading, the shock and vibration bulletin 2: isolation and damping, impact, blast. Washington DC, The Shock and Vibration Information Center; 1978. p. 115–22.
[10] Lavoie MA, Gakwaya A, Nejad Ensan M, Zimcik DG. Validation of available approaches for numerical bird strike modeling tools. Int Rev Mech Eng 2007;v1(4):380–9.
[11] Lavoie MA, Gakwaya A, Nejad Ensan M, Zimcik DG, Nandlall D. Bird substitutes tests results and evaluation of available numerical methods. Int J Impact Eng 2009;36(10):1276–87.
[12] Liu G, Li Y, Gao X. Bird strike on a flat plate, experiments and numerical simulations. Int J Impact Eng 2014;70:21–37.
[13] Cook SS. Erosion by water-hammer. Proceedings of the royal society of London, series A. 119. 1928. p. 481–8.
[14] Hopkins HG, Kolsky H. Mechanics of hypervelocity impact of solids. Proceedings of the fourth symposium on hypervelocity impact, paper no. 12. Air Force Proving Ground Center, Eglin Air Force Base, Florida; 1960.
[15] Dear JP, Field JE. High-speed photography of surface geometry effects in liquid/solid impact. J Appl Phys 1988;63:1015–21.
[16] Field JE, Dear JP, Ogren JE. The effects of target compliance on liquid drop impact. J Appl Phys 1989;65:533–40.
[17] Field JE, Lesser MB, Dear JP. Studies of two-dimensional liquid-wedge impact and their relevance to liquid-drop impact problems. Proc R Soc Lond A 1985;401:225–49.
[18] Field JE, Camus JJ, Tinguely M, Obreschkow D, Farhat M. Cavitation in impacted drops and jets and the effect on erosion damage threshold. Wear 2012;290:154–60.
[19] Heymann FJ. On the shock wave velocity and impact pressure in high-speed liquid-

solid impact. J Basic Eng 1968;90:400–2. Transactions of the ASME, series d
[20] Johnson W, Vickers GW. Transient stress distribution caused by water jet impact. J Mech Eng Sci 1973;15(4).
[21] Bowden FP, Brunton JH. The deformation of solids by liquid impact at supersonic speeds. Proceedings of the Royal Society, London, Series A. vol. 263. 1961. p. 433–50.
[22] Brunton JH. The physics of impact and deformation: single impact. Philos Trans R SocLond, A 1966;260:73–85.
[23] Bowden FP, Field JE. The brittle fracture of solids by liquid impact, by solid impact and by shock. Proceedings of the royal society of london, series A. 263. 1964. p. 331–52.
[24] Glenn LA. On the dynamics of hypervelocity liquid jet impact on a flat rigid surface. J Appl Math Phys (ZAMP) 1974;25:383–98.
[25] MATLAB. Version R2013b (8.20.701). The MathWorks Inc., Natick, MA; 2013.
[26] Leissa AW. The free vibration of rectangular plates. J Sound Vib 1973;31:257–93.
[27] Leissa AW. Vibration of plates. NASA Report SP-160. Ohio State University, Columbus, OH; 1969.
[28] Wu JH, Liu AQ, Chen HL. Exact solutions for free-vibration analysis of rectangular plates using bessel functions, ASME. J Appl Mech 2007;74:1247–51.
[29] Aarnes TE. Study of the natural frequencies of a disc. Norwegian University of Science and Technology, Trondheim, Norway; 2015. Msc thesis, ept-m-2014-157.
[30] Savitzky A, Golay MJE. Smoothing and differentiation of data by simplified least squares procedures. Anal Chem 1964;36(8):1627–39.
[31] Acharya D, Rani A, Agarwal S, Singh V. Application of adaptive Savitzky-Golay filter for EEG signal processing. Perspectives in science. 8. Elsevier; 2016. p. 677–9.
[32] Cooper PW. Explosives engineering. VCH, New York; 1996.
[33] Carlucci DE, Jacobson SS. Ballistics: theory and design of guns and ammunition. CRC Press, Taylor and Francis Group, LLC, Boca Raton, FL; 2008.
[34] Alekseevskii P. Penetration of a rod into a target at high velocity. Combust Explos Shock Waves 1966;2:63–6.
[35] Tate A. A theory for the deceleration of long rods after impact. J Mech Phys Solids 1967;15:387–99.
[36] Walters WP, Segletes SB. An exact solution of the long rod penetration equations. Int J Impact Eng 1991;11(2):225–31.
[37] Segletes SB, Walters WP. Efficient solution of the long-rod penetration equations of Alekseevskii-Tate. US Army Research Directorate, AMSRL-WM-TD, Aberdeen Proving ground, MD; 2002. Arl report arl-tr-2855.
[38] Walters WP, Williams C. A solution of the Alekseevskii-Tate equations. US Army Research Directorate, AMSRL-WM-TD, Aberdeen Proving ground, MD; 2005. Arl report arl-tr-3606.
[39] Flis WJ. Modified alekseevskii-tate model for rod penetration of porous targets. Proceedings of the 28thinternational symposium on ballistics, Edinburgh, Scotland, UK. 2016. p. 2219–27.
[40] Cronin DS, Falzon C. Characterization of 10% ballistic gelatine to evaluate temperature, aging and strain rate effects. J Exper Mech 2011;51:1197–206.
[41] Winter J, Shifler D. The material properties of gelatine gels. Ballistic Research Laboratories, Aberdeen Proving Ground, MD; 1975. Ballistic research laboratories report AD-a008 396, Brl contractor report no. 217.

DOCUMENT CONTROL DATA

*Security markings for the title, authors, abstract and keywords must be entered when the document is sensitive

1. ORIGINATOR (Name and address of the organization preparing the document. A DRDC Centre sponsoring a contractor's report, or tasking agency, is entered in Section 8.) DRDC - Valcartier Research Centre Defence Research and Development Canada 2459 route de la Bravoure Quebec (Quebec) G3J 1X5 Canada	2a. SECURITY MARKING (Overall security marking of the document including special supplemental markings if applicable.) CAN UNCLASSIFIED 2b. CONTROLLED GOODS NON-CONTROLLED GOODS DMC A

3. TITLE (The document title and sub-title as indicated on the title page.)

On the determination of the shock and steady state parameters of gelatine from cylinder impact experiments

4. AUTHORS (Last name, followed by initials – ranks, titles, etc., not to be used)

Nandlall, D.; Gakwaya, A.

5. DATE OF PUBLICATION (Month and year of publication of document.)	6a. NO. OF PAGES (Total pages, including Annexes, excluding DCD, covering and verso pages.)	6b. NO. OF REFS (Total references cited.)
May 2018	33	41

7. DOCUMENT CATEGORY (e.g., Scientific Report, Contract Report, Scientific Letter.)

External Literature (P)

8. SPONSORING CENTRE (The name and address of the department project office or laboratory sponsoring the research and development.)

DRDC - Valcartier Research Centre
Defence Research and Development Canada
2459 route de la Bravoure
Quebec (Quebec) G3J 1X5
Canada

9a. PROJECT OR GRANT NO. (If appropriate, the applicable research and development project or grant number under which the document was written. Please specify whether project or grant.) Soldier System Effectiveness (SoSE) peoject	9b. CONTRACT NO. (If appropriate, the applicable number under which the document was written.)
10a. DRDC PUBLICATION NUMBER (The official document number by which the document is identified by the originating activity. This number must be unique to this document.) DRDC-RDDC-2018-P069	10b. OTHER DOCUMENT NO(s). (Any other numbers which may be assigned this document either by the originator or by the sponsor.)

11a. FUTURE DISTRIBUTION WITHIN CANADA (Approval for further dissemination of the document. Security classification must also be considered.)

Public release

11b. FUTURE DISTRIBUTION OUTSIDE CANADA (Approval for further dissemination of the document. Security classification must also be considered.)

12. KEYWORDS, DESCRIPTORS or IDENTIFIERS (Use semi-colon as a delimiter.)

Low strength material impact, Soft body material impact, shock pressure of gelatin impact, bird impact loading, bird strike, impact and shock loading to human surrogate materials, shock pressure from force history

13. ABSTRACT/RÉSUMÉ (When available in the document, the French version of the abstract must be included here.)

For a soft body projectile striking a target or the shock loading of a soft body material, the determination of the interface shock pressure, shock speed and applied steady state pressures is important but has been hindered by technical challenges even with the use of sophisticated embedded pressure sensors in the target surface. Difficulties interpreting the results render the accuracies sometimes questionable or impossible to reproduce. Here we propose a simple impact experiment using a force sensor and an analysis procedure to derive the interface pressure from the force/time history. The results are compared to those obtained from shock Hugoniot and penetration equations. We came upon the presence of a dynamic pressure that is significantly higher than the expected stagnation pressure. This method could be used to determine and characterise the shock and steady state pressures of a wider range of materials under impact and shock loading conditions.